Dataset of lava samples, melt and fluid inclusions analysis from the Virunga Volcanic Province (DR Congo) (https://doi.org/10.5880/fidgeo.2024.029)

Boudoire Guillaume[1]

1. *Université Clermont Auvergne, CNRS, IRD, OPGC, Laboratoire Magmas et Volcans, Aubière, France*

1. Licence

2. Citation

When using the data please cite:

Boudoire, Guillaume (2024): Dataset of lava samples, melt and fluid inclusions analysis from the Virunga Volcanic Province (DR Congo). GFZ Data Services. https://doi.org/10.5880/fidgeo.2024.029

The data are supplementary material to:

Boudoire G., Bobrowski N., Burgi P.-Y., Calabrese S., France L., Giuffrida G., Grassa F., Karume K., Kazadi Mwepu J.-C., Kuhn J., Moritz R., Munguiko Munyamahoro O., Rizzo A. L., Tedesco D. (submitted). Magmatic activity in incipient continental break-up as revealed by coupling melt and fluid inclusions. Journal of Petrology – Letters.

Table of contents

3. Data Description

A field campaign was performed in 2020 to sample eruptive products in the Virunga Volcanic Province (Democratic Republic of Congo) to investigate the chemical composition and the barometry of melt and fluid inclusions. The related dataset (.xls) is composed by seven spreadsheets: (1) lava samples analysis (name, location, composition in major elements by ICP-AES), (2) fluid inclusions barometry (CO_2 density by microthermometry and Raman spectroscopy), (3) fluid inclusions chemistry (noble gases and carbon isotopes by mass spectrometry), (4) shrinkage bubble composition in melt inclusions (CO_2 content by Raman spectroscopy), (5) glass composition in melt inclusions (major elements by EPMA, trace elements by LA-ICP-MS, and volatile elements by SIMS), (6) reconstructed and corrected composition of melt inclusions (by using the MIMiC software), (7) input parameters used for degassing models paths (by using Solex and SulfurX softwares). The full description of the data and methods is provided in the data description file.

3.1. Analytical Procedure

3.1.1. Bulk rock

Major element chemistry from five whole rocks was obtained by using Inductively Coupled Plasma Atomic Emission Spectroscopy (ICP-AES) at the Laboratoire Magmas et Volcans (Aubière, France). Lava samples were powdered and mixed with $LiBO_2$ before melting in an induction oven at 1050 °C for 4.5 min, using graphite crucibles. The glass beads obtained were then dissolved in a solution of deionized water and nitric acid (HNO_3). Finally, solutions were diluted by a factor of 2000 before analysis with a HORIBA-Jobin-Yvon ULTIMA C. Relative uncertainty (2σ) on major elements is 1.5 % for Al_2O_3, 1.9 % for SiO_2, 2.7 % for MgO, 3.1 % for Na_2O, 3.1 % for CaO, 3.2 % for Fe_2O_{3T}, 3.5 % for K_2O, 4.0 % for TiO_2, 4.8 % for MnO, and 4.9 % for P_2O_5, on average. Description of the sample and data are fully available in the "2024-029_Boudoire_Data.xlsx" file.

3.1.2. Fluid inclusions and shrinkage bubbles

Fluid inclusions were studied in polished handpicked olivine and clinopyroxene crystals from crushed lava samples. Early recognition of secondary and pseudo-secondary fluid inclusions (Goldstein and Reynolds, 1994) was made by optical microscopy at the Laboratoire Magmas et Volcans (Aubière, France).

CO_2 densimetry and barometric estimates

Microthermometry was carried out at the Department of Earth Sciences of the University of Geneva (Geneva, Switzerland) by using a Linkam TMH 600 heating and freezing stage operating with a thermal resistor and liquid nitrogen, respectively. The stage is mounted on a DMLB Leica microscope with a maximum objective of 100x connected to a JVC camera. Calibration was made on synthetic fluid inclusions standards of pure CO_2 and H_2O. Melting (Tm) and homogenisation (Th) temperature were reproducible to ±0.1 °C with a manually controlled heating rate in the range of 0.2-0.5 °C/min during phase transition. Freezing temperature was operated down to -120 °C. Melting temperature was measured at -56.9 °C for the few fluid inclusions where the transition was viewable, i.e., similar to the melting point of pure CO_2 fluid inclusions at -56.6 °C. Clathrates were not observed and homogenisation systematically occurred to liquid phase. Subsequent CO_2 density in fluid inclusions were calculated from the homogenization temperatures by using the equation of state of Span and Wagner (1996). Uncertainty of CO_2 density by microthermometry is lower than 0.007 cc/g in this study.

Additionally, CO_2 density in 5 fluid inclusions and 17 shrinkage bubbles in melt inclusions were analysed by Raman spectroscopy for calculations of CO_2 densities from the Fermi dyad split between the 1388 and 1285 cm^{-1} peaks (Frezzotti et al., 2012). The protocole applied for fluid inclusions preparation is similar to that described in Boudoire et al. (2023). Measurements were performed at the Laboratory Magmas et Volcans (Aubière, France) by using an inVia confocal Raman micro-spectrometer manufactured by Renishaw. The micro-spectrometer was equipped with a 532 nm diode laser (200 mW output power), a Peltier-cooled CCD detector of 1040 x 256 pixels, and a Leica DM 2500 M optical microscope with a motorized XYZ stage. Laser power was periodically checked and reduced to 1.8 and 3.1 mW on the sample surface. A 100x microscope objective, a 20 μm slit aperture, and a grating of 2400 grooves/mm were used leading to a spectral resolution better than 0.4 cm^{-1}, and spatial resolutions of 1 μm (lateral) and 2-3 μm (vertical) near the surface. Calibration of the wavelength was performed based on the 520.5 cm^{-1} peak of Si. The spectra were recorded with the WiRETM 4.2 software in a single window collection (recommended by Lamadrid et al. (2017) for CO_2 densimetry) of 365-1575 cm^{-1} to cover the vibrational frequencies of mineral phases (host crystals, carbonates, sulphates) and gaseous phases (CO_2-SO_2). The two Neon emission lines at ~ 17347.803 and 17575.260 cm^{-1} (absolute wavenumber), which brackets the Fermi dyad, have been collected over several months of measurements, resulting in a linearity correction factor (Lamadrid et al., 2017) ranging between 0.9990 and 1.0006. It leads to an uncertainty on the calculated CO_2 density, σ(splitting), lower than 0.037 g/cc. Three to four Raman spectra were acquired (two at 1.8 mW and two at 3.1 mW) to test the reproducibility of the analyses, σ(reproducibility), for each single fluid inclusion or shrinkage bubble. The equation of Song et al. (2009) was identified as the most reliable for the instrument at the Laboratoire Magmas et Volcans with a deviation on internal standards, σ(equation), not exceeding 0.037 g/cc of CO_2 (Boudoire et al., 2023). The uncertainty related to the spectral resolution by peak fitting, σ(processing), is lower than 0.014 g/cc (Kobayashi et al., 2012). Finally, the total uncertainty, σ(TOT) on CO_2 density related to the use of the CO_2 densimeter of Song et al. (2009) and to the analytical conditions is:

$$\sigma(TOT) = \sqrt{\sigma(splitting)^2 + \sigma(reproducibility)^2 + \sigma(equation)^2 + \sigma(processing)^2}$$

In this study σ(TOT) is equal to 0.055 g/cc for fluid inclusion and lower than 0.066 g/cc for shrinkage bubble. The use of Raman spectroscopy at room temperature for the evaluation of CO_2 density from the Fermi dyad is not applicable between 0.22 and 0.74 g/cc (coexistence of gas and liquid CO_2). In this study, the CO_2 density of fluid inclusions analyzed by Raman spectroscopy range between 0.77 and 0.94 g/cc and are not concerned with this fact. Only 3 shrinkage bubbles present an apparent CO_2 density above 0.22 g/cc. They were discarded in the calculations of the initial CO_2 content dissolved in melt inclusions.

Pure CO_2 shrinkage bubbles were analyzed whereas the presence of calcite (Raman peak at 1085 cm^{-1}) and anhydrite (Raman peak at 1018 cm^{-1}; Frezzotti et al., 2012) was sometimes evidenced in fluid inclusions. This observation points to the presence of a CO_2-H_2O initial mixture (Boudoire et al., 2021, 2023). In agreement with previous inferences made on CO_2-H_2O initial mixture in fluid inclusions analyzed in other similar studies (Hansteen and Klügel, 2008; Zanon and Frezzotti, 2013), we consider an upper limit of 10 % mol of H_2O in the initial exsolved phase. Such value leads to a maximum increase of density of 0.03 g/cc. Pressure from CO_2 density in fluid inclusions was estimated with the ISOC code (Bakker, 2003) using the equation of state of Duan et al. (1992, 1996) set for CO_2-H_2O mixture on a large range of pressure and temperature. The average temperature estimated from the corrected composition of melt inclusions (see below) was used for each eruptive site: 1229 °C at Rumoka, 1183

°C at Mudjoga, and 1259 °C at Kashaka. Any uncertainty on temperature results only in minor errors on pressure (35 MPa for a maximum standard deviation on temperature estimated from melt inclusions of 86 °C). Finally, in this study, the cumulated uncertainty on pressure estimates from CO_2 densimetry in fluid inclusions does not exceed 52 and 76 MPa from microthermometry and Raman spectroscopy, respectively. Data are fully available in the "2024-029_Boudoire_Data.xlsx" file.

Noble gases and carbon isotopes

Helium (^{3}He, ^{4}He), neon (^{20}Ne), argon (^{40}Ar, ^{38}Ar, ^{36}Ar), and carbon (^{13}C/^{12}C noted as δ^{13}C versus VPDB reference in per mil) isotopes were measured at the Istituto Nazionale di Geofisica e Vulcanologia (INGV) - Sezione di Palermo (Italy). Measurements were performed in the gas phase entrapped in fluid inclusions hosted in minerals. In detail, 0.3-0.9 g of crystals (among olivine, clinopyroxene, and nepheline) were hand-picked for noble gas measurements, while about 1.0 g of clinopyroxene and olivine crystals was used for CO_2 extraction and carbon isotope measurements (without residual glass around the crystals). Then, crystals were cleaned in an ultrasonic bath and loaded in two distinct single-step crushers for the noble gas and CO_2 extraction from fluid inclusions, following the protocols reported in Rizzo et al. (2018) and Sandoval-Velasquez et al. (2022). After purification and separation of distinct species with cryogenic techniques, He and Ne isotopes were analysed using two distinct split-flight-tube mass spectrometers (Helix SFT-Thermo), and Ar isotopes using a multi-collector mass spectrometer (Argus, GVI). Typical blanks for He, Ne, and Ar were $<10^{-15}$, $<10^{-16}$, and $<10^{-14}$ mol, respectively. The analytical uncertainties (1σ) for ^{3}He/^{4}He are <6 % (and mostly <2 %).

The gas mixture trapped as fluid inclusions (primarily CO_2) was released by single-step crushing the crystals at a pressure of approximately 200 bar. This gas mixture was then purified using a Pyrex glass line, and the CO_2 was quantified manometrically using a 626B Baratron® Absolute Capacitance Manometer MKS. After purification, the CO_2 was trapped in a glass sampler, adjusted to atmospheric pressure by adding pure helium. The sampler was subsequently transferred to a Thermo (Finnigan) Delta Plus XP CF-IRMS, which was connected to a Trace GC gas chromatograph and a Thermo (Finnigan) GC/C III interface, to determine the ^{13}C/^{12}C ratios. The analytical error (1σ) is approximately 0.3‰.

Measured ^{3}He/^{4}He were corrected for atmospheric contamination based on their ^{4}He/^{20}Ne and the values are expressed as Rc/Ra (Ra = ^{3}He/^{4}He in air) with:

$$R_c = \frac{(R_m \times \left({}^{4He}/_{20Ne}\right)_m - R_a \times \left({}^{4He}/_{20Ne}\right)_a)}{(\left({}^{4He}/_{20Ne}\right)_m - \left({}^{4He}/_{20Ne}\right)_a)}$$

where R_m and $(^4He/^{20}Ne)_m$ are the measured values, and R_a and $(^4He/^{20}Ne)_a$ refers to the atmospheric value (0.318; Ozima and Podosek, 2002). ^{40}Ar was also corrected for the atmospheric contamination, as follows:

$$40Ar^* = 40Ar_m - (36Ar_m \times \left({}^{40Ar}/_{36Ar}\right)_a)$$

where ^{40}Ar* is the corrected value, $^{40}Ar_m$ the measured value, and $(^{40}Ar/^{36}Ar)_a$ = 298.56 (Lee et al., 2006).

In total, 12 analyses of noble gases were performed (on distinct mineral phase aliquots) corresponding to 5 eruptive products (Nyiragongo, Nyamulagira, Mudjoga, Kashaka, and Rumoka). Due to analytical

limits due to the minimum amount of CO_2 required to perform $\delta^{13}C$ measurements, 3 analyses of carbon isotopes were performed (Rumoka and Kashaka), only. Two measurements of noble gases (nepheline aliquot from Nyiragongo and olivine aliquot from Nyamulagira) were discarded from the dataset because of evidence of noble gases diffusion across the crystals ($^3He/^4He$ decrease correlated to lower ^3He content and lower $^4He/^{40}Ar^*$; Yamamoto et al., 2009; Boudoire et al., 2020). Data are fully available in the "2024-029_Boudoire_Data.xlsx" file.

3.1.3. Melt inclusions

Glassy melt inclusions were found in olivine and nepheline crystals from 2020 lavas emitted at Nyamulagira and Nyiragongo, respectively. All melt inclusions in olivine crystals from Rumoka, Kashaka, and Mudjoga lavas were crystalline and were subsequently homogenized on a Vernadsky-style heating stage mounted under a microscope at the Laboratoire Magmas et Volcans (Aubière, France) (Figure 1). The homogenization was carried out at 1 atm in a bath of purified helium kept at oxygen fugacity between 10^{-10} and 10^{-9} atm. The temperature was raised from room temperature to liquidus temperature within a span of 20 min, monitored with a thermocouple, and then quenched (Le Voyer et al., 2008). Homogenization temperatures were in the range 1260-1290 °C, 1240-1270 °C, and 1270-1300 °C for Mudjoga, Kashaka, and Rumoka products, respectively. These temperatures are close to the temperatures estimated from the whole rock chemistry by the use of the MgO-thermometer of Putirka (2008). This procedure should not result in measurable H_2O-loss from the inclusions during (Gaetani et al., 2012). Melt inclusions were individually exposed using silicon carbide paper, followed by polishing using a 0.3 µm alumina paste. Crystal-hosted melt inclusions were finally pressed into an aluminum mount filled with indium.

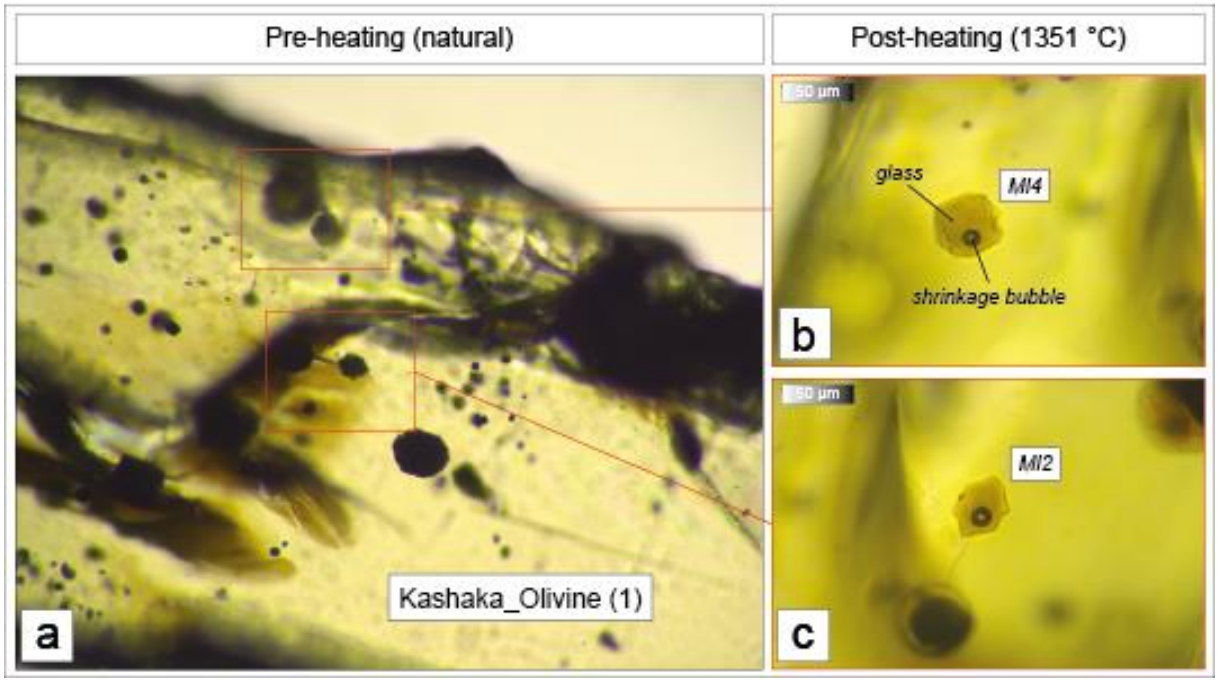

Figure 1: (a) Photomicrographs of crystalized melt inclusions entrapped in an olivine crystal (from Kashaka lava) and (b, c) homogenized melt inclusions obtained after heating at 1351 °C. Homogenized melt inclusions are systematically composed by a glassy part and a shrinkage bubble.

Major and trace elements

Electron microprobe analyses were performed using a Cameca SXFive at the Laboratoire Magmas et Volcans (Aubière, France) operated with a 15 kV accelerating voltage and (1) a 20 nA current focused beam with a 15 μm-diameter spot for mineral analysis and (2) an 8 nA current focused beam with a 10 μm-diameter spot for melt inclusions. Uncertainty (1σ) on forsteric content of olivine is lower than 0.57. Relative uncertainty (1σ) on major elements is 0.6 % for Al_2O_3, 0.7 % for SiO_2, 0.8 % for CaO, 1.3 % for MgO, 1.8 % for K_2O, 1.8 % for FeO, 2.2 % for Na_2O, 2.7 % for TiO_2, 8.4 % for P_2O_5, and 15.9 % for MnO, on average.

Trace elements (La, Ce, Pr, Nd, Sm, Eu, Dy, Er, Yb, Y, Zr, Hf, Nb, Ta, V, Th, U, Pb, Ba, Sr, Rb, Sc, Co, Li) were analysed at the Laboratoire Magmas et Volcans (Aubière, France) by Laser Ablation (LA) using a 193 nm ArF excimer laser system (Resonetics M50) with a Thermo Fisher Element XR Inductively Coupled Plasma Mass Spectrometry (ICP-MS) with helium as carrier gas. Laser repetition of 1 Hz and a 20 μm-diameter spot were used. The background was measured for 30 s before ablation and acquisition during 90 s. Calibration was made on BCR and GSD standards using CaO as the internal reference element. The relative uncertainty (1σ) on standards ranged from 0.7 to 12.4 % for all considered elements, on average. Data are fully available in the "2024-029_Boudoire_Data.xlsx" file.

Volatiles

Dissolved CO_2, H_2O, S, F, and Cl contents in melt inclusions were quantified by Secondary Ion Mass Spectrometry (SIMS). SIMS analyses were performed using a CAMECA 1280 HR2 SIMS at the CRPG-CNRS (Nancy, France). A Cs+ primary Gaussian beam of 0.8 nA accelerated at 10 kV was focused to a 15-μm-wide spot size. A normal-incidence electron gun was used for charge compensation. Pre-sputtering was performed for 90 s over a 15 × 15 μm area to remove any remaining carbon contamination. Negative secondary ions ^{12}C, ^{17}O, $^{16}O^1H$, ^{18}O, ^{19}F, ^{27}Al, ^{30}Si, ^{32}S, and ^{35}Cl were measured in mono-collection mode at a mass resolution of 7,500 in order to separate ^{17}O from $^{16}O^1H$, $^{29}Si^1H$ on ^{30}Si, $^{31}P^1H$ on ^{32}S and $^{34}S^1H$ on ^{35}Cl peaks. An energy slit of 30 eV was used without energy offset. The sample chamber vacuum was kept below 2×10^{-9} torr using a liquid nitrogen trap. Measurements were conducted by ion counting on electron multipliers (EM) for ^{12}C, ^{17}O, ^{19}F, ^{32}S, and ^{35}Cl, and on faraday cups (FC2) with 1012 ohm resistors for $^{16}O^1H$, ^{18}O, ^{19}F, and ^{30}Si. Each analysis consisted of 8 scans, with counting times of 4 s per scan on each peak, and waiting times of 1 s for EM measurements and 5 s for FC2 measurements. Data from samples that failed to produce a stable signal during the analysis were discarded and are not reported. The uncertainty relative to the instrumental conditions is defined as σ(instrument) in the following. Because the instrumental mass fractionation (IMF) depends on Si and alkaline contents (Hauri et al., 2002), analyses of volatile contents (especially CO_2 and H_2O) by SIMS must use suitable standards with a composition close to that of the sample. Basalt (M34, M35, M43, M48, 40428, 47963, KL2G, VG2, KE12; Shishkina et al., 2010; Binderman et al., 2012; Sobolev et al., 2016), nephelinite (MELI-4, MELI-7, MELI-8, MELI-10: Mourey et al., 2023), and phonolite (in-house CRPG standards Phono0, Phono7, Phono9; Mollex, 2017) standards with variable H_2O, CO_2, S, F, and Cl contents were used (Table 1). The nephelinite standards were used for CO_2 and H_2O at Nyiragongo, Nyamulagira, Kashaka, and Mudjoga (whole rock chemistry closer to the nephelinite standard) whereas the basalt standards were used for CO_2 and H_2O at Rumoka. The basalt standards were used for S, Cl, F determination in all the samples. The signal was normalized to ^{18}O rather than ^{30}Si to minimize the silica composition dependence of the analysis (Figure 2). The linear regression calibration lines display a R-squared greater than 0.95 (Figure 2). In order to take into account the uncertainty on the equations of calibrations, we simulated 1000 random sampling (Monte Carlo method) for each analysis. The final deviation standard on the 1000 numerical results was considered as representative

of the uncertainty on the linear regression, σ(equation). Additionally, we considered another uncertainty related to the chemical deviation between the selected set of standards (basalt or nephelinite) and the sample, σ(standard):

$$\sigma(standard) = K \times (value_{calibration1} - value_{calibration2})$$

Where $value_{calibration1}$ is the obtained value for a volatile component based on the most adapted set of standards (1), $value_{calibration2}$ is the value obtained by using another set of standards (2) whose the chemistry is in line with the sample and the set of standards (1), and K is the percentage of contribution of the set of standards (2) on the chemistry of the sample with respect to the set of standards (1). The total uncertainty, $\sigma(TOT)$, was calculated for each analysis and for each volatile compounds following the equation:

$$\sigma(TOT) = \sqrt{\sigma(instrument)^2 + \sigma(equation)^2 + \sigma(standard)^2}$$

For our samples, the averaged total uncertainty is 0.17 wt% for H_2O, 1451 ppm for CO_2, 208 ppm for F, 112 ppm for S, and 123 ppm for Cl, on average. High uncertainty is mostly viewable for the melt inclusions from 2020 Nyiragongo products for which the chemical composition is the furthest from the set of standards.

Table 1: Composition of the glass standards (in wt% excepting for CO2, S, F, Cl in ppm) used for SIMS calibration.

Standard	Na_2O	MgO	CaO	K_2O	TiO_2	FeO	SiO_2	Al_2O_3	CO_2	H_2O	S	F	Cl
M34	2.25	6.29	10.15	0.23	0.85	8.67	46.00	16.60	375	5.70	-	-	-
M35	2.28	6.50	10.11	0.23	0.84	8.26	45.96	16.83	1019	4.20	-	-	-
M43	2.27	6.65	10.59	0.23	0.88	8.82	47.46	17.21	3172	2.62	-	-	-
M48	2.39	6.26	11.40	0.24	0.91	7.93	49.33	17.85	176	0.77	-	-	-
40428	3.10	6.84	10.84	0.58	1.68	9.10	50.40	25.89	-	0.85	890	650	4940
47963	4.24	5.90	10.85	1.76	1.91	6.81	48.18	18.17	-	1.45	776	777	1356
KL2G	2.35	7.34	10.90	0.48	2.56	10.70	50.30	13.30	-	-	7.7	177	26
VG2	2.62	6.71	11.12	0.19	1.85	11.84	50.81	14.06	153	0.28	1424	300	298
KE12	7.28	0.00	0.35	4.27	0.33	8.36	70.30	7.62	-	-	210	4200	3280
MELI-4	2.47	17.79	12.38	1.21	4.22	7.80	43.53	10.59	9840	1.45	-	-	-
MELI-7	2.47	17.79	12.38	1.21	4.22	7.80	43.53	10.59	20920	1.77	-	-	-
MELI-8	2.47	17.79	12.38	1.21	4.22	7.80	43.53	10.59	15650	2.69	-	-	-
MELI-10	2.47	17.79	12.38	1.21	4.22	7.80	43.53	10.59	13320	0.32	-	-	-
Phono0	10.69	0.40	1.98	8.24	1.01	7.89	54.34	15.26	100	0.00	-	-	-
Phono7	10.69	0.40	1.98	8.24	1.01	7.89	54.34	15.26	1500	4.03	-	-	-
Phono9	10.69	0.40	1.98	8.24	1.01	7.89	54.34	15.26	7100	1.63	-	-	-

The CO_2 content in shrinkage bubbles (Figure 1) was calculated from the CO_2 density measured by Raman spectroscopy (d_{CO2}; see above) using the formula of Hartley et al. (2014):

$$CO2\ (ppm) = 10^6 \times \frac{d_{CO2} \times V_{sh}}{d_{glass} \times V_{glass}}$$

Where V_{sh} is the volume of the shrinkage bubble on the basis of a sphere (diameter measured by microscopy), V_{glass} is the volume of glass in the melt inclusions on the basis of an ellipsoid (axis a, b, and c measured by microscopy), and d_{glass} is the glass density. As the potential irregularity of the melt inclusion may lead to a significant uncertainty on the estimation of the volume of the melt inclusion, an error of ±10% was considered in the calculations following previous inferences (Hartley et al., 2014). Except for one melt inclusion, the ratio between the volume of the shrinkage bubble and the volume of the melt inclusion range between 1.1 and 5.3 %. These values are fully consistent with previous results obtained for other volcanic provinces (Hanyu et al., 2020; Boudoire et al., 2021). Shrinkage bubbles in melt inclusions hosted in nepheline crystals from the 2020 Nyiragongo lava were systematically empty. Glass density was approximated with the density of respective whole rock samples based on the model of Lange and Carmichael (1987) considering the chemical composition, the temperature, and the pressure (with similar input parameters than those used for the calculation of the oxygen fugacity described below). Data are fully available in the "2024-029_Boudoire_Data.xlsx" file.

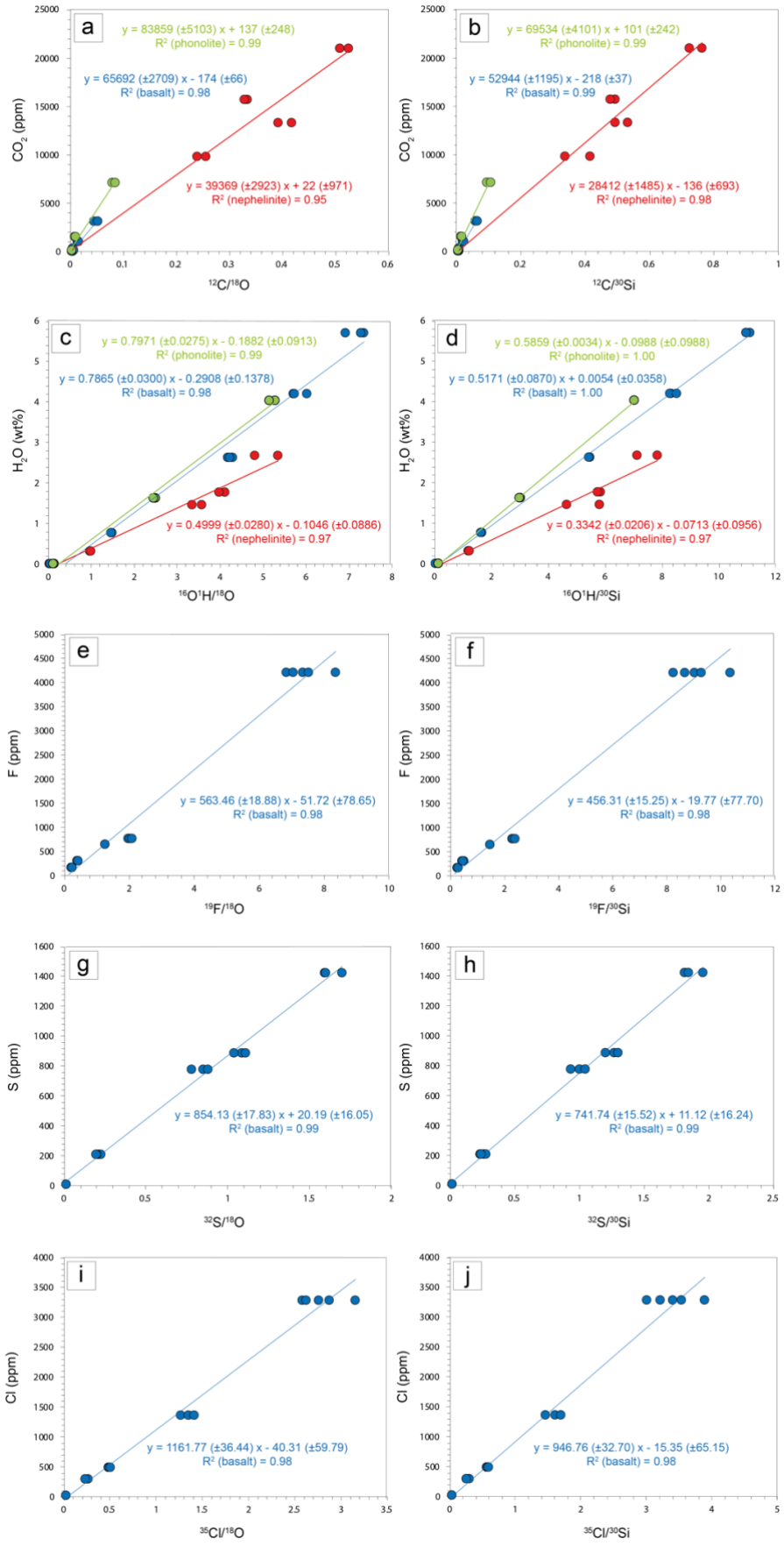

Figure 2: Calibration curves (CO2-H2O-S-Cl-F) at the SIMS obtained for basaltic, nephelinitic, and phonolitic melt compositions.

Correction of melt inclusions and barometry

Melt inclusions may be affected by post-entrapment processes as crystallisation of the host crystal and Fe-loss (see Rose-Koga et al. (2021) for a complete review). Melt inclusions in in nepheline crystals (4 melt inclusions) were not corrected due to the absence of correction models. However, melt inclusions whose the composition evolves on a liquid line of descent opposite to the host crystal (and thus suspected to be affected by post-entrapment crystallisation process, PEC, as evidenced on some BSD images at the EPMA; Figure 3) were excluded from the dataset. Melt inclusions in olivine crystals (15 melt inclusions) were corrected using the MIMiC Python program (Rasmussen et al., 2020). In addition to the measured composition of melt inclusions, input parameters required estimates of (1) the Fe^{3+}/Fe^{TOT} in liquid, (2) the initial FeO_T content, and (3) the forsterite content of the host olivine crystal. (1) Oxygen fugacity and Fe^{3+}/Fe^{TOT} in liquid were estimated (Kress and Carmichael, 1991) from previous chemical analysis of whole rocks where Fe_2O_3 and FeO were measured. Only lavas with a composition similar to our samples were considered: 6 lavas emitted between 1967 and 1982 at Nyamulagira (Aoki, 1985), 9 lavas emitted in 1977 and 2022 at Nyiragongo (Nakamura, 1980; Platz et al., 2004), the alkali basalt '96.615' (Platz et al., 2004) for Rumoka, and the rushayite '2' (Denaeyer, 1966) for Kashaka and Mudjoga. The temperature used for calculations of oxygen fugacity was estimated from the MgO content of bulk rocks (Putirka, 2008) and a pressure range from 1 to 10,000 bar was considered to obtain an averaged value. At Nyiragongo and Nyamulagira, estimated oxygen fugacities (see Excel dataset) are consistent with the ones measured by Morrison et al. (2020). (2) The initial FeO_T content was considered equal to that of the whole rock analysis. (3) The forsterite content of the host olivine crystals was calculated from EPMA analysis with an uncertainty (1σ) of 0.55 on Fo. Two correction models were tested: (*Model 1*) PEC only, and (*Model 2*) PEC and Fe-loss. Results from the *Model 1* were not considered reliable for two reasons: (1) corrected MgO and FeO_T content of melt inclusions are not consistent with previous results obtained for similar products (Rumoka and Nyamulagira) by Head et al. (2011), and (2) estimated entrapment temperature of melt inclusions are strongly lower (<1200 °C) than homogenisation temperature obtained with the heating stage (>1240 °C). More consistent results are obtained by using the *Model 2*. A range of -10.5 % to 15.7 % olivine was added during the correction that overlaps the one obtained by Head et al. (2011) for melt inclusions at Nyamulagira.

The initial CO_2 content in melt inclusions (with the total uncertainty calculated from SIMS and Raman analysis; see above) was used for barometric estimates. H_2O-CO_2 solubility models lack calibration experiments for basanitic and foiditic melts (see Iacovino at al., 2021). Consequently, we used the CO_2 solubility model of Eguchi and Dasgupta (2018) for barometric estimates. This model is best suited for alkaline melt composition with H_2O content lower than 3 wt% as the products analyzed in our study. A crustal density of 2.8 (Campbell and Davis, 2017) was used for the conversion of barometric estimates in depth estimates. Data are fully available in the "2024-029_Boudoire_Data.xlsx" file.

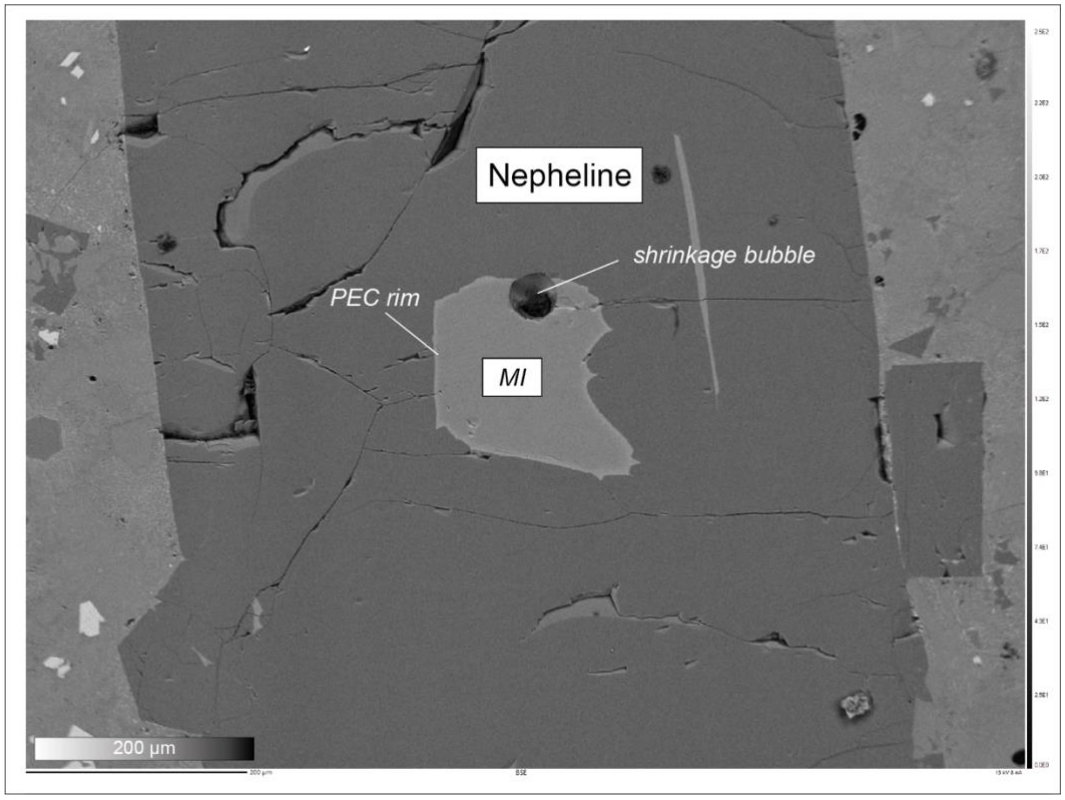

Figure 3: BSE imagery of a melt inclusion entrapped in a nepheline crystal from Nyiragongo lava. Chemical heterogeneity is evidenced by the presence of a post-entrapment crystallisation rim. These kind of melt inclusions entrapped in nepheline crystals were systematically discarded from the final dataset.

3.1.4. Degassing models

Starting from the composition of melt inclusions in volatile elements at both Nyiragongo and Nyamulagira, we modeled the expected evolution of CO_2/SO_2 and Cl/S in the exsolved gas phase as a function of the pressure. Among all the magmatic degassing models present in literature, we used both SolEx (Witham et al., 2012) and SulfurX (Ding et al., 2023) that are currently the best-suited CO_2-S-Cl degassing models for pressures lower than 400 MPa (see Ding et al. (2023) for a review). In our case, limitations about SolEx expecting results mainly raise on the choice of the sulfur partition coefficient between the vapor and the melt, the absence of oxygen fugacity changes by S degassing and S-Fe electron exchange during the modeling, and the absence of H_2S partitioning that required to conduct runs at NNO >0.5 (Witham et al., 2012). SulfurX model is expected to overcome these issues but was mainly developed for basalt and basaltic andesite magmas and not for basanite (Nyamulagira) and nephelinite (Nyiragongo) melts. To limit this effect, the model of Nash et al. (2019) for Fe-S speciation in the melt was implemented in the runs. This model is based on natural alkaline mafic melts, rather than on irrelevant (in our case) calc-alkaline (Muth and Wallace, 2021) or experimental (O'Neill and Mavrogenes, 2022) melts. As the thermodynamic model of Nash et al. (2019) is more temperature-dependent than the other models, we have tested the effect of an uncertainty of 50°C on the initial temperature of the melts. This uncertainty overlaps temperature estimates before the onset of rapid crystallization for Nyiragongo and Nyamulagira melts (Morrison et al., 2020), previous estimates using geothermometers (Burgi et al., 2018, 2021) and the uncertainty on the use of the glass thermometers of Putirka (2008) to estimate the temperature of melt inclusions based on their composition. Runs were conducted by considering both Fractional Equilibrium Degassing (FED) and Batch Equilibrium Degassing (BED) possibilities. Comparative results between SolEx and SulfurX CO_2/SO_2 degassing paths are shown in Figure 4 and confirm that SolEx model is not suited for this study.

At Nyiragongo, an averaged composition of melt inclusions in nepheline crystals was used. Due to apparent H_2O-loss in the melt inclusions analysed in our study, an initial value of 0.65 wt% was considered (Burgi et al., 2014). Initial temperature, pressure and oxygen fugacity were determined by following the methodology described above. At Nyamulagira, we considered two distinct initial liquids: one relative to the most magnesian melt inclusion (also characterized by the highest pressure) and one representative of the rest of the dataset (less magnesian and lower pressure). Due to apparent H_2O-loss in the melt inclusions analysed in our study with respected to previous analyses documented in literature, we fixed an initial value of 1 wt% corresponding to the average obtained by Head et al. (2011). Initial temperature, pressure and oxygen fugacity were determined by following the methodology described above. Starting conditions used for the modeling are fully available in the "2024-029_Boudoire_Data.xlsx" file.

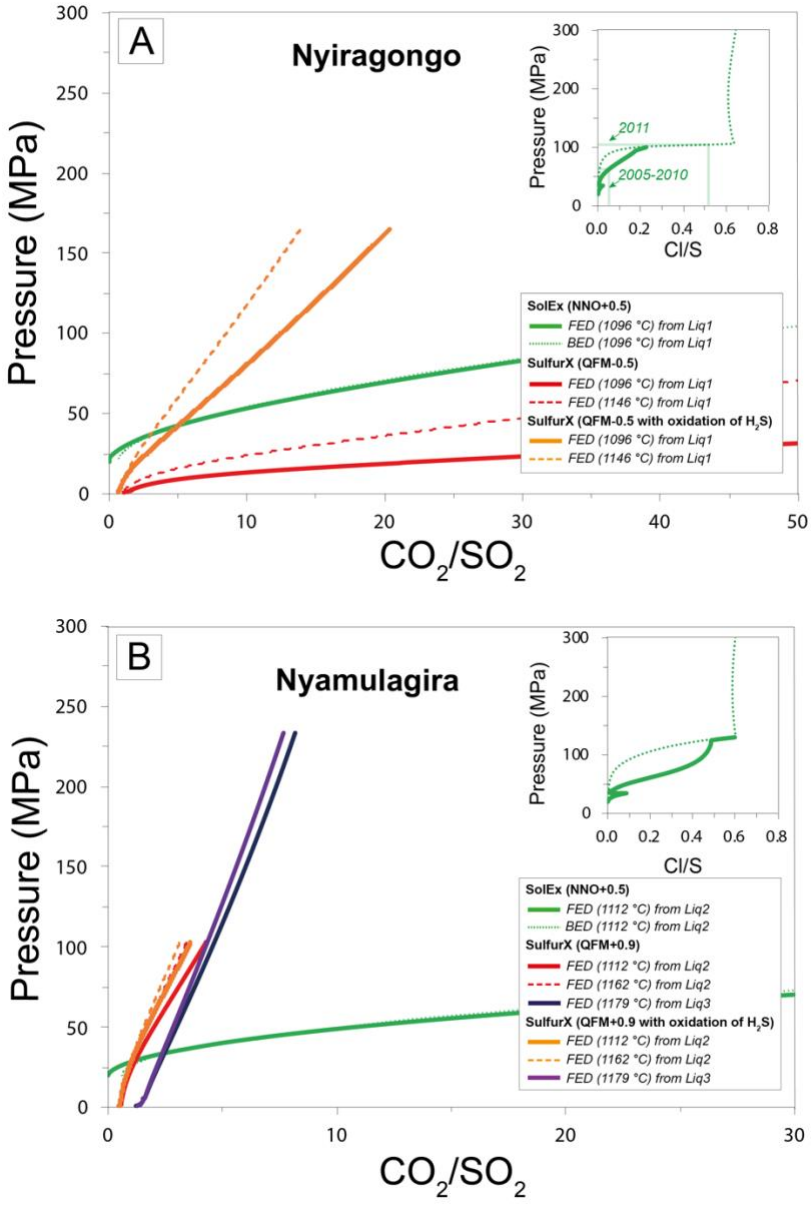

Figure 4: Comparison between SolEx and SulfurX degassing models at (a) Nyiragongo and (b) Nyamulagira under variable starting conditions described in the text.

4. File description

4.1. File inventory

The zipped folder contains the data description ("2024-029_Boudoire_Data-Description.pdf") and the data represented in one Excel file ("2024-029_Boudoire_Data.xlsx") and seven tab delimited txt files corresponding to the different Excel sheets.

The data file(s) report(s) the full dataset through seven spreadsheets: (1) "Bulk rock" for lava samples analysis (name, location, composition in major elements), (2) "Fluid inclusions (Barometry)" for fluid inclusions barometry (CO_2 density), (3) "Fluid inclusions (Noble gases)" for fluid inclusions chemistry (noble gases and carbon isotopes), (4) "Melt inclusions (Bubble)" for shrinkage bubble composition in melt inclusions (CO_2 content), (5) "Melt inclusions (Glass)" for glass composition in melt inclusions (major, trace, and volatile elements), (6) "Melt inclusions (Corrected)" for reconstructed and corrected composition of melt inclusions (by using the MIMiC software), and (7) "Degassing models" for input parameters used for degassing models paths (by using Solex and SulfurX softwares).

4.1.1. 2024-029-Boudoire_Data

Table 2: File 2024-029-Boudoire_Data.xlsx contains analysis of bulk rocks, fluid inclusions, melt inclusions, and input parameters for degassing modelling.

Column header	unit	Description
Samples		Samples are identified by group (Nyiragongo volcano, Nyamulagira volcano, Peripheral cones) and name. For fluid inclusions the host mineral is added as well as the label of the fluid inclusion analysed in a crystal and the number of reiterated analysis (for noble gases). For melt inclusion the host crystal is added as well as the label of the melt inclusion in the same crystal.
Coordinates	XXXXXX and XXXXXXX	Latitude in m S and Longitude in m E (Mercator system)
Long	DD,dddd	Longitude in m E (Mercator)
Composition in major elements	wt%	Value of SiO_2, TiO_2, Al_2O_3, FeO_T, CaO, MgO, MnO, Na_2O, K_2O, P_2O_5 and Total in wt%
Classification		Nomenclature of the lava type according Pouclet et al. (2016) based on the bulk rock composition in major elements
Calculations - Estimations	°C and without unit	Estimations of the temperature in °C, of the oxygen fugacity (QFM, NNO), and of the Fe^{3+}/Fe_T ratio from bulk rock analysis (see 2024-029-Boudoire_Data-Description.pdf for the calculations)
Microthermometry	°C and g/cc	Homogenisation temperature in °C and corresponding CO_2 density in g/cc
Raman spectroscopy	cm^{-1} and g/cc	Fermi dyad in cm^{-1} and corresponding CO_2 density in g/cc
Barometry from CO_2 densimetry	g/cc, °C, and MPa	Final density (CO_2+H_2O) of the fluid inclusions in g/cc, averaged entrapment temperature of the corresponding melt inclusions in °C, and corresponding calculated pressure in MPa (see 2024-029-Boudoire_Data-Description.pdf for the calculations)
Gas content	mol/g	^4He, ^3He, CO_2, ^{40}Ar, ^{38}Ar, ^{36}Ar, $^{40}Ar^*$ content in mol/g in the gas entrapped in fluid inclusions and released by crystal crushing. 1σ for the standard deviation on the measurement.
Isotopic ratios	‰ and without unit	$^4He/^{40}Ar^*$, R/Ra, Rc/Ra, $^{40}Ar/^{36}Ar$, $CO_2/^3He$, $\delta^{13}C$ in the gas entrapped in fluid inclusions and released by crystal crushing. 1σ for the standard deviation on the measurement. "-" stands for the absence of analysis.

Column header	unit	Description
Melt inclusion	μm and μm^3	Length of ellipsoid axes of the melt inclusions in μm and related volume in μm^3
Shrinkage bubble	μm, μm^3, cm^{-1}, g/cc, ppm	Diameter of the spherical shrinkage bubble in μm, related volume in μm^3, ratio of the bubble on melt inclusion volume, Fermi dyad in cm^{-1} in the shrinkage bubble with the uncertainty σ in cm^{-1}, corresponding CO_2 density in the shrinkage bubble in g/cc, glass density of the melt inclusion in g/cc, induced CO_2 content in the shrinkage bubble with the uncertainty σ in ppm (see 2024-029-Boudoire_Data-Description.pdf for the calculations)
Volatile elements	ppm	H_2O, CO_2, F, S, Cl content dissolved in the glass of melt inclusions in ppm. CO_2(TOT) in ppm is the reconstructed CO_2 content by adding the CO_2 in the glass with the CO_2 of the shrinkage bubble. Analytical uncertainty in ppm (1σ)
Trace elements	ppm	Values of La, Ce, Pr, Nd, Sm, Eu, Dy, Er, Yb, Y, Zr, Hf, Nb, Ta, V, Th, U, Pb, Ba, Sr, Rb, Sc, Co, Li content in melt inclusions.
MIMiC calculations	°C, MPa and without unit	PEC percentage (post-entrapment crystallisation), Kd (equilibrium coefficient between the melt inclusion and the host crystal), estimated temperature of the melt inclusions in °C from MIMiC calculations (Rasmussen et al., 2020). Entrapment pressure in MPa from the CO_2 solubility model of Eguchi and Dasgupta (2018) and related standard deviation (1σ) (see 2024-029-Boudoire_Data-Description.pdf for the calculations)
Temperature-pressure-redox conditions	°C, MPa and without unit	Temperature in °C, pressure in MPa and oxygen fugacity (QFM buffer) with the uncertainty (1σ) used as input parameters for the degassing modelling (see 2024-029-Boudoire_Data-Description.pdf for the calculations)

In the "Melt inclusions (Glass)" and "Melt inclusions (Corrected)" spreadsheets, a terminal row entitled

"Averaged 1σ" define the averaged analytical uncertainty for each element for the full dataset.

5. References

Eguchi, J., & Dasgupta, R. (2018). A CO_2 solubility model for silicate melts from fluid saturation to graphite or diamond saturation. Chemical Geology, 487, 23-38. https://doi.org/10.1016/j.chemgeo.2018.04.012

Pouclet, A., Bellon, H., & Bram, K. (2016). The Cenozoic volcanism in the Kivu rift: Assessment of the tectonic setting, geochemistry, and geochronology of the volcanic activity in the South-Kivu and Virunga regions. Journal of African Earth Sciences, 121, 219-246. https://doi.org/10.1016/j.jafrearsci.2016.05.026

Rasmussen, D. J., Plank, T. A., Wallace, P. J., Newcombe, M. E., & Lowenstern, J. B. (2020). Vapor-bubble growth in olivine-hosted melt inclusions. American Mineralogist, 105(12), 1898-1919. https://doi.org/10.2138/am-2020-7377